Bendola Publishing
Journal of Transition Metal Complexes
Vol. 3 (2020), Article ID 246114, 11 pages
doi:10.32371/jtmc/246114

Research Article

Spectroscopic and Theoretical Studies of Some Bivalent Metal Complexes of a Quinoline Schiff Base Derivative

Ramadan M. Ramadan,[1] Rania G. Mohamed,[2] Mona Hassan,[2] and Samir M. El-Medani[2]

[1]*Chemistry Department, Faculty of Science, Ain Shams University, Cairo 11566, Egypt*
[2]*Chemistry Department, Faculty of Science, Fayoum University, Fayoum 63514, Egypt*
Address correspondence to Samir M. El-Medani, samirmedani20@gmail.com

Received 27 November 2020; Revised 14 December 2020; Accepted 15 December 2020

Abstract Interaction of M(II) ions, M=Co, Ni, Cu, Zn, and Pd, with a Schiff base ligand (HL), derived from the condensation of 2-hydroxy-5-nitrobenzaldehyde and 8-aminoquinoline, gave the complexes $[Co(L)_2(H_2O)_2]$, $[Ni(L)_2(H_2O)_2]$, $[Cu(L)(H_2O)]CH_3COO$, $[Zn(L)(H_2O)]CH_3COO$, and $[Pd(HL)Cl_2]$. The ligand and its complexes were characterized by means of elemental and thermal analyses, molar conductance, and magnetic moment measurements along with the different spectroscopic techniques. Theoretical calculations based on DFT were carried out to verify the optimized structures of ligand and complexes. The relative reactivity of the compounds was estimated from chemical descriptors analysis using the HOMO and LUMO frontier orbitals. Molecular docking of ligand and its zinc complex revealed that the interaction of Zn(L) with DNA is comparable to that of HL due to the presence of water OH groups instead of the hydroxyl group of ligand.

Keywords copper complexes; X-ray analysis; DFT studies; antioxidant activity; CT-DNA binding; molecular docking

1. Introduction

In the last few decades, Schiff base derivatives showed a vital importance in the chemistry of organic and coordination compounds [1,2,3,4]. These compounds stemmed their significance from their applications as models in biology, medicinal, and bioinorganic chemistry [5,6], as well as their uses in industrial catalysis, corrosion, and photochromism [7,8,9]. In addition, photo- and thermochromic properties of the Schiff bases and their metal complexes make them significant in modern technology. They are found to be valuable in optical computers to measure and control of the radiation of imaging systems, in the molecular memory storages and photo detectors in biological systems [10]. Moreover, heterocyclic Schiff bases containing one or more nitrogen atoms are considered as good ligands. This is due to the presence of nitrogen atoms in the rings with a localized pair of electrons [11,12,13]. In particular, the quinoline framework containing Schiff base derivatives were found to serve as important heterocyclic compounds with diverse array of biological properties, such as anti-asthmatic, anti-bacterial, and anti-inflammatory agents [14, 15]. Moreover, the quinolines occurred as based natural products as quinine and chloroquine, which have been extensively used as drugs for the treatment of malaria [16]. Also, the chloro-aminoquinoline Schiff base derivatives were screened for their anticholinesterase activity, which assessed for Alzheimer disease [17]. The inhibitory activity of these compounds and their copper derivatives was evaluated by Ellman's spectrophotometric method in acetylcholinesterase (ACHE) and butyrylcholinesterase (BCHE) from equine serum. Docking and molecular dynamics studies of ACHE were performed and the results suggested that these compounds are able to bind inside ACHE similarly to other inhibitors [17]. On the other hand, many studies of mixed ligand complexes with nitrogen-containing heterocyclic derivatives (such as 8-hydroxyquinoline and 2-aminothiazole) and the corresponding Schiff base ligands were reported. These derivatives have interesting structural features and in vitro antimicrobial and cytotoxicity activities [18]. It was found that the presence of aromatic and/or heteroaromatic groups in the structure of nitrogen gives these ligands additional properties and therapeutic, pharmacologic, and DNA cleavage activity [19,20].

On continuation of our interest in synthesis and investigations of many Schiff base ligands and their transition metal complexes [2,4,21,22,23], here we report the synthesis of a Schiff base derived from the condensation of 2-hydroy-5-nitro benzaldehyde and 8-aminoquinoline as well as its Co(II), Ni(II), Cu(II), Zn(II), and Pd(II) complexes. Different spectroscopic tools, biological activities along with DFT calculations and molecular docking were used to characterize the ligand and the complexes.

2. Experimental

2.1. Reagents

$CoCl_2 \cdot 6\,H_2O$, $Ni(CH_3COO)_2 \cdot 4\,H_2O$, $Cu(CH_3COO)_2 \cdot H_2O$, $Zn(CH_3COO)_2 \cdot 2\,H_2O$, and dichloro-1,5-cyclooctadienepalladium, 2-hydroy-5-nitro benzaldehyde and

Table 1: Color, yield, elemental analyses, and mass spectra data for the reported compounds.

Compound	Chemical formula	Color	Yield (%)	Elemental analyses, found (calcd.)			Mass spectra		μ_{eff} BM	Molar conduct. Ω^{-1} mol^{-1} cm^2
				C (%)	H (%)	N (%)	MW	m/z		
HL.H_2O	$C_{16}H_{13}N_3O_4$	Orange	82	61.03 (61.73)	3.72 (4.21)	13.37 (13.50)	311.30	294 $[P-H_2O]^+$	—	—
$[Co(L)_2(H_2O)_2]$	$C_{32}H_{24}N_6O_8Co$	Brown	57	57.35 (56.56)	3.37 (3.56)	12.32 (12.37)	679.51	680 $[P]^+$	3.74	8
$[Ni(L)_2(H_2O)_2]$	$C_{32}H_{24}N_6O_8Ni$	Dark orange	63	57.35 (56.58)	3.37 (3.56)	12.32 (12.37)	679.28	680 $[P]^+$	2.80	6
$[Cu(L)(H_2O)]CH_3COO$	$C_{18}H_{15}N_3O_6Cu$	Dark brown	65	51.83 (49.94)	3.41 (3.49)	10.07 (9.71)	432.88	374 $[P-CH_3COO]^+$	1.40	8
$[Zn(L)(H_2O)]CH_3COO$	$C_{18}H_{15}N_3O_6Zn$	Light yellow	77	49.59 (49.73)	3.06 (3.48)	9.94 (9.67)	434.72	376 $[P-CH_3COO]^+$	—	7
$[Pd(HL)Cl_2]$	$C_{16}H_{11}N_3O_3Cl_2Pd$	Dark brown	58	41.16 (40.84)	2.66 (2.36)	6.32 (8.93)	470.59	471 $[P]^+$	—	6

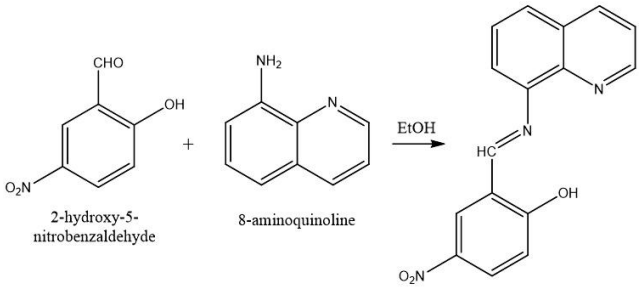

Scheme 1: Synthesis of HL.

8-aminoquinoline were purchased from Aldrich. All solvents were of analytical grade and purified by distillation.

2.2. Instruments

IR spectra (KBr pellets) were recorded on a Unicam-Mattson 1000 FT-IR spectrometer. NMR measurements were performed on a Varian Mercury VX-300 NMR spectrometer. Samples were dissolved in DMSO-d_6. Magnetic susceptibilities of the paramagnetic complexes in the solid state (Gouy method) were measured on a Sherwood Scientific magnetic susceptibility balance. Conductivity measurements were carried out in DMSO (1×10^{-3} M) at 25 °C using Jenway 4010 conductivity meter. Mass spectra of the solid complexes (70 eV, EI) were performed on a Finnigan MAT SSQ 7000 spectrometer. Bruker EMX spectrometer was used to record the electron spin resonance spectra at 25 °C in the X-band frequency 9.714 GHz, and on a microcrystalline powder with microwave power around 2.012 mW. Thermogravimetric analyses were carried out under nitrogen atmosphere with a heating rate of 10 °C/min using a Schimadzu DT-50 thermal analyzer. Elemental analyses were performed on a Perkin-Elmer 2400 CHN elemental analyzer.

2.3. Synthesis of (E)-4-nitro-2-((quinolin-8-ylimino)methyl)phenol (HL) ligand

The Schiff base ligand was synthesized by refluxing a mixture of 2-hydroy-5-nitro benzaldehyde (1.67 g, 10 mmol) and 8-aminoquinoline (1.44 g, 10 mmol) in 25 mL absolute ethanol for 3 h. The reaction mixture was cooled and the solvent was evaporated. The residue obtained was washed using cold ethanol, and then recrystallized from hot ethanol. A crystalline orange product was left to dry for few hours (yield 83%), Scheme 1.

2.4. Synthesis of metal complexes

A general procedure was employed to synthesize the reported metal complexes. A 1:1 molar ratio from the ligand and metal salt was used except for the cobalt and nickel complexes (1:2 metal to ligand). The reaction mixture in methanol was refluxed for 3 h until the color was changed. The solution was left to stand overnight. The residue was separated by filtration, washed with hot petroleum ether, and then recrystallized from hot ethanol. The fine crystals formed were left to dry under vacuum for several hours. Table 1 gives the color, yield, elemental analyses, and mass spectral data of the reported compounds.

2.5. Biological activity

In vitro antibacterial and antifungal activity of the ligand and its complexes were tested against four bacteria: *Escherchia coli* and *Enterobacter aerogenes* as Gram-negative bacteria and *Staphylococcus aureus* and *Enterococcus faecalis* as Gram-positive bacteria, and the fungus: *Aspergillus niger*. The tests were carried out using paper disc diffusion method (The Central lab, Cairo University, Egypt). The detailed procedure was previously reported [2, 21]. The obtained data for antibacterial were compared with those of doxycycline as an antibacterial standard.

Table 2: Assignments of the important experimental and calculated vibrational modes and ^{1}H NMR data of HL ligand.

Experimental IR (cm^{-1})*	Calculated frequencies	Intensity	Assignment	^{1}H NMR data (ppm)
3,431 (s,b)	—	—	νOH (water of crystallization)	10.31 s (OH), 9.54 s (HC=N),
2,920 (m)	2,507	85	νOH	9.06–8.03 m (quinoline ring),
—	1,681	25	νR, δOH, νC=N	7.81–6.86 (phenyl ring)
—	1,661	8	νC=$N_{quinoline}$, νR	
—	1,651	21	νR, νC=$N_{azomethine}$	
1,623 (s)	1,628	10	νR, νC=$N_{quinoline}$, νC=$N_{azomethine}$	
1,542 (m)	1,559, 1,553	10, 6	νR, δOH	
1,437 (m)	1,470, 1,446	10, 7	δCH, νC−O, $\nu_{sym}(NO_2)$	
1,238 (m)	1,276	50	δCH, νC−O, $\nu_{sym}(NO_2)$	
826 (mw)	820	11	νR, $\delta_{scissor}(NO_2)$	

*ν, stretch; δ, in-plane bend; m, medium; s, strong; b, broad; mw, medium weak.

2.6. Computational details

All the calculations were performed using the hybrid density functional theory (DFT) method B3LYP as implemented in the Gaussian 09 software package [24]. The geometries were optimized using the standard double zeta plus polarization basis set 6-31G (d,p) for the ligand atoms and effective core potential basis set LANL2DZ for the metal complexes. The purpose of the quantum mechanics calculations validates the proposed 3D structure of the obtained compounds as well as to find out key factors for their reactivity. The theoretical calculations of the spectral modes of vibrations of ligand were carried out using DFT.

2.7. Molecular docking

The docking studies were performed using AutoDock Vina 4 [25]. Two macromolecule targets (PDB ID: 4MZI and 1ZEW) were used for docking the ligand and its zinc complex. 4MZI is a p53 tumor suppressor protein, which is the most frequently mutated gene in human cancer [26]. 1ZEW is an X-ray crystal structure of a B-DNA of inverted repeat DNA sequence d(CCnnnN6N7N8GG), where N6, N7, and N8 are naturally occurring nucleotides [27]. The molecular visualization system PyMOL (2.0.7) was used to visualize the docking molecules [28].

3. Results and discussion

Interaction of the quinoline derivative Schiff base ligand HL (Scheme 1) with the bivalent cobalt and nickel ions resulted in the formation of neutral octahedral complexes with the molecular formula $[M(L)_2(H_2O)_2]$. On the other hand, reactions of Cu^{2+} and Zn^{2+} ions with HL gave the two cationic complexes $[M(L)(H_2O)]CH_3COO$. In case of the reaction of $PdCl_2$ with HL, the neutral complex $[Pd(HL)Cl_2]$ was formed without the loss of ligand proton. The ligand and its metal complexes were characterized using different spectroscopic techniques (IR, ^{1}H NMR, mass), elemental analyses, magnetic measurements, molar conductance, and thermal analysis. Elemental analyses and mass spectra data of the reported compounds were in accordance with the proposed molecular formulas. The molar conductivities of 1×10^{-3} M solutions of the complexes at 25 °C were found to be in the range 11–16 Ω^{-1} mol^{-1} cm^2 (Table 1) indicating non- or weak electrolyte characteristics of these derivatives. The magnetic susceptibility measurements for the cobalt, nickel, and copper paramagnetic complexes at 298 K gave effective magnetic moment (μ_{eff}) values in accordance with the corresponding unpaired electrons, Table 1. The observed small deviation from the spin-only moments could be due to the spin-orbit coupling.

3.1. Spectral studies

The IR spectra (KBr pellets) of the ligand and its complexes were recorded in the region 4000–400 cm^{-1}. The most prominent IR and ^{1}H NMR spectral data for HL and complexes are given in Tables 2 and 3. The experimental and calculated vibrational modes of HL were investigated to assign and compare the modes of the important functional groups such as ν(OH), ν(C=N), and $\nu(NO_2)$ [2]. The IR spectrum of HL displayed a strong and broad band due to νOH. The shift of the band towards lower frequency than those of usual free OH groups could be owing to the existence of hydrogen bond between hydroxyl proton and the azomethine nitrogen. Also, the spectrum exhibited two medium stretching frequency bands at 1,437 cm^{-1} and 1,238 cm^{-1} due to asymmetric and symmetric νNO_2. The ^{1}H NMR spectrum of HL in deuterated DMSO showed a slightly broad singlet at 10.31 ppm, which is assigned to the hydroxyl proton. This signal disappeared on addition of D_2O to solution. The spectrum also displayed a singlet due to the azomethine proton and two multiples for the quinoline and phenyl rings, Table 2. The IR spectra of the reported metal complexes showed the functional groups of the ligand, such as C=N and NO_2 groups, with the appropriate shift due to complex formation, Table 3. Interestingly, except for the palladium complex, the IR spectra of the other complexes showed the disappearance of OH band. It indicated that the ligands coordinated to metal from the hydroxyl oxygen and the azomethine nitrogen [2,

Table 3: IR and NMR data for the reported complexes.

Complex	IR data (cm^{-1})*				^{1}H NMR data (ppm)
	υ(OH)	υ(C=N)	υ(C=C)	υ(NO_2)	
$[Co(L)_2(H_2O)_2]$	3,436 (m,b)	1,605 (s)	1,539 (m)	1,404 (m)	—
			1,454 (m)	1,239 (m)	
$[Ni(L)_2(H_2O)_2]$	3,437 (m,b)	1,606 (s)	1,539 (m)	1,403 (m)	—
			1,484 (m)	1,237 (m)	
$[Cu(L)(H_2O)]CH_3COO$	3,436 (m,b)	1,611 (s)	1,545 (m)	1,402 (m)	—
			1,506 (m)	1,239 (m)	
$[Zn(L)(H_2O)]CH_3COO$	3,431 (m,b)	1,611 (s)	1,543 (sh)	1,407 (m)	9.54 s (HC=N), 8.89–8.05 m (quinoline ring),
			1,474 (m)	1,238 (m)	7.90–6.68 (phenyl ring)
$[Pd(HL)Cl_2]$	3,133 (m,b)	1,601 (s)	1,544 (m)	1,385 (m)	12.20 b,s (OH), 10.23 s (HC=N), 8.43–7.92 m
			1,505 (m)	1,232 (m)	(quinoline ring), 7.72–6.92 (phenyl ring)

*m, medium; s, strong; b, broad; sh, shoulder.

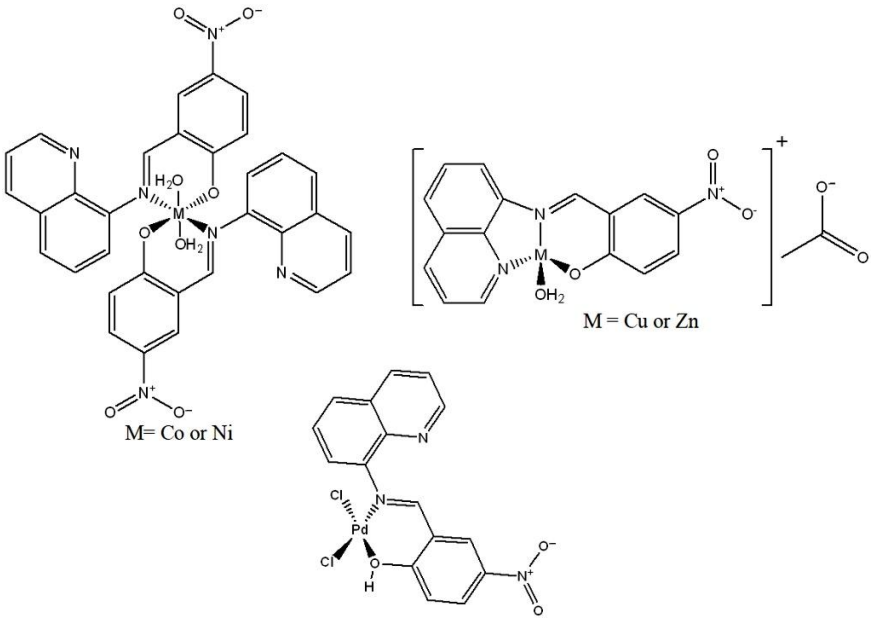

Scheme 2: The proposed structures of complexes.

21,22,23]. The shifts in the bands of the other functional groups, towards low frequencies, also confirmed such a conclusion. Furthermore, the IR spectra of the complexes displayed new nonligand bands corresponding to stretching frequencies of the M−O and M−N moieties [29]. The ^{1}H NMR spectra for the zinc and palladium complexes gave more insight to their structures. It is worth to mention that the NMR spectrum of the palladium complex displayed a broad singlet at 12.20 ppm for the hydroxyl hydrogen. This signal was shifted to lower energy relative to that of ligand (10.31 ppm). Scheme 2 gives the proposed structures of the isolated complexes.

Electron spin resonance (ESR) is a powerful tool for investigating the structure and dynamics of molecular systems containing paramagnetic center. The ESR spectrum of the microcrystalline powder copper complex, $[Cu(L)(H_2O)]CH_3COO$, was recorded at room temperature on the Klystron X-band at frequency 9.714 GHz, and with microwave power around 2.012 mW and the g factors were measured relative to the standard indicator DPPH ($g = 2.0037$); see Figure 1. The ESR signals in parallel and perpendicular regions appeared as partially resolved signal due to either distortion in geometry or electron-spin-nuclear-spin coupling. The spectrum of the complex displayed a $g_{\|}$ value $= 2.065$, while the $g_{\perp}$ value $= 2.095$. According to Kivelson and Neiman, the $g_{\|}$ value in the Cu(II) complex can be used as a measure of covalent characteristics of the metal-ligand bond [30]. For the ionic case, the $g_{\|}$ value is generally ≥ 2.3, while for covalent state it is < 2.3. Since the value of $g_{\|}$ of the complex is smaller than 2.3, the Cu(II)-ligand bonds have a considerable covalent property. The observed values for g, where $g_{\perp} > g_{\|} > 2.003$, indicated that the unpaired electron is mainly localized in the d_{z_2} orbital of the copper(II) ion [31]. The geometric factor G is a measure of exchange interaction between the copper centers in the solid compounds. The G factor can be calculated using the

expression [32]:

$$G = \left(g_{\parallel} - 2.0023\right)/\left(g_{\perp} - 2.0023\right).$$

If the value of G is larger than 4, the exchange interaction between copper(II) centers is considered negligible. On the other hand, if G is smaller than 4, a significant exchange interaction can be specified in the complex. The calculated G factors for the present complexes are 0.68 indicating a significant exchange interaction between the copper ions.

The electronic absorption spectrum of HL in either MeOH or CH_2Cl_2 consists of a UV band (π–π^*) and two broad bands in the visible region, Table 4. The position of the UV band was not changed in the two solvents. The lower wavelength bands correspond to n–π^* transitions. This showed a little red shift in CH_2Cl_2 relative to that in methanol. On the other hand, the other visible band (higher wavelength) showed a corresponding red shift in CH_2Cl_2 solvent with respect to that of methanol one, Table 4. This absorption band could be due to a charge transfer (CT) between HL and the solvent. Obviously, the CT is stronger in case of methanol solvent [33,34]. The spectra of the complexes also displayed two absorption bands for π–π^* and n–π^* transitions with the appropriate shift due to complex formation (Table 4). The two complexes, Cu(L) and Zn(L), showed a shoulder to the UV band. Interestingly, the spectra of the complexes did not exhibit CT bands, presumably because the two sites expected to involve the CT (OH and HC=N) were engaged in the coordination.

3.2. Thermal analysis

In order to give more insight into the structure of the complexes, thermal studies on the solid complexes using TG and differential thermogravimetric (DTG) techniques were performed [35]. The TG and DTG plots of $[Co(L)_2(H_2O)_2]$, $Co[C_{32}H_{24}N_6O_8]$; MW = 679.51, exhibited four decomposition steps. The first from 125–350 °C, with a net weight loss of 5.30 (5.25) %, is probably due to elimination of two coordinated H_2O; see Table 5. The second step occurred in the temperature range 350–450 with a net weight loss of 22.66%, which is consistent with elimination of ($C_{10}H_4NO$). The third in the temperature range 350–450 with a net weight loss of 10.89% corresponding to elimination of (C_3H_8NO). The fourth step ranged from 647 °C to 1,000 °C to give finally solid residual of CoO + 4C (Table 5). The TG and DTG plots of $[Ni(L)_2(H_2O)_2]$, $Ni[C_{32}H_{24}N_6O_8]$; MW = 679.28, exhibited four decomposition steps in the temperature range 130–1,000 °C. The first step (130–300 °C) showed mass percent of 5.30% which corresponded to elimination of two H_2O. The second, third, and fourth steps at temperature ranges 300–426 °C, 426–609 °C, and 609–1,000 °C showed the elimination of mass percent of

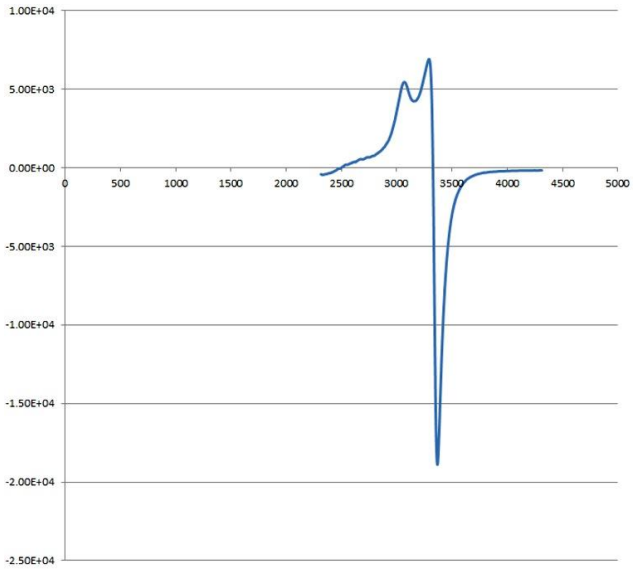

Figure 1: Radiograph of lap joint defects.

24.14%, 17.37%, and 38.57% corresponding to $C_9H_{10}NO_2$, $C_6H_2N_2O$, and $C_{15}H_8N_3O_2$ species, respectively, leaving finally NiO + 2C solid species (Table 5). Thermal studies of the copper complex, $[Cu(L)(H_2O)]CH_3COO$, were carried out using thermogravimetry. The TG plot of $Cu[C_{18}H_{13}N_3O_5]$; MW = 414.868 showed two well defined and nonoverlapping steps in the 216–1,000 °C range (listed in Table 5). The first at 216–477 °C showed a net weight loss of 38.87% corresponding to elimination of $C_7H_6N_2O_3$. The second decomposition peak (477–1,000 °C) showed a net weight loss of 29.95% corresponding to a residual solid of CuO + 5C (Table 5). The TG and DTG plots of $[Zn(L)(H_2O)]CH_3COO$, Zn $[C_{18}H_{15}N_3O_6]$; MW = 434.723, exhibited three decomposition steps. The first from 120–300 °C, with a net weight loss of 14.72%, is probably due to elimination of one coordinated H_2O and CH_4NO species; see Table 5. The second step occurred in the temperature range 300–400 with a net weight loss of 4.37%, which is consistent with elimination of (H_3O) species. The third in the temperature range 400–1,000 with a net weight loss of 56.59% corresponding to elimination of ($C_{15}H_6N_2O_2$) to give finally a solid residual of ZnO + 2C (Table 5).

The TG and DTG plots of $[Pd(HL)Cl_2]$; $Pd[C_{16}H_{11}N_3O_3Cl_2]$; MW = 470.58, required three decomposition steps. The first from 50–309 °C, with a net weight loss of 15.09%, is probably due to elimination of Cl_2 molecule (Table 5). The second step occurred in the temperature range 309–454 with a net weight loss of 28.69%, consistent with elimination of ($C_7H_9N_3$). The third in the temperature range 454–1,000 with a net weight loss of 24.22% corresponding to elimination of (C_8H_2O) to give finally solid residual of PdO_2 + C (Table 5).

Table 4: The UV-vis data of HL and its complexes.

Compound	UV-vis data (nm)	
	MeOH	CH_2Cl_2
HL	232 (π–π^*), 325 (n–π^*), 440 (CT)	230 (π–π^*), 328, 455 (CT)
$[Co(L)_2(H_2O)_2]$	233 (π–π^*), 310 (n–π^*)	230 (π–π^*), 300 (n–π^*)
$[Cu(L)(H_2O)]CH_3COO$	225 (π–π^*), 254 (π–π^*), 334 (n–π^*)	231 (π–π^*), 260 (π–π^*), 335 (n–π^*)
$[Zn(L)(H_2O)]CH_3COO$	229 (π–π^*), 253 (π–π^*), 330 (n–π^*)	230 (π–π^*), 260 (π–π^*), 320 (n–π^*)
$[Pd(HL)Cl_2]$	234 (π–π^*), 310 (n–π^*)	245 (π–π^*), 283 (n–π^*)

Table 5: Thermogravimetric data of (HL) ligand and its Co(II), Ni(II), Cu(II), Zn(II), and Pd(II) complexes.

Complex	Decomp. step (°C)	Mass loss (%)	MW loss		Species eliminated	Solid residue (%)
		Found (Calcd.)	Found	Calcd.		Found (Calcd.)
$[Co(L)_2(H_2O)_2]$	125–350	5.30 (5.25)	36	35.7	$2H_2O$	(CoO + 4C)
	350–450	22.66 (22.64)	154	153.84	$C_{10}H_4NO$	18.09 (18.26)
	450–647	10.89 (10.99)	74	74.68	C_3H_8NO	
	647–1,000	42.97 (42.86)	292	291.23	$C_{15}H_8N_4O_3$	
$[Ni(L)_2(H_2O)_2]$	130–300	5.30 (5.281)	36	35.87	$2H_2O$	(NiO + 2C)
	300–426	24.14 (24.219)	164	164.52	$C_9H_{10}NO_2$	14.528 (14.50)
	426–609	17.37 (17.50)	118	118.88	$C_6H_2N_2O$	
	609–1,000	38.57 (38.50)	262	261.53	$C_{15}H_8N_3O_2$	
$[Cu(L)(H_2O)]CH_3COO$	216–477	38.87 (38.47)	—	166.14	$C_7H_6N_2O_3$	(CuO + 5C)
	477–1,000	29.95 (29.41)	166.51	127.31	$C_6H_9NO_2$	32.23 (32.12)
$[Zn(L)(H_2O)]CH_3COO$	120–300	14.72 (14.68)	64	63.55	$H_2O + CH_4NO$	(ZnO + 2C)
	300–400	4.37 (4.382)	19	19.05	H_3O	24.243 (24.21)
	400–1,000	56.59 (56.79)	246	246.6	$C_{15}H_6N_2O_2$	
$[Pd(HL)Cl_2]$	50–309	15.09 (15.159)	71	71.34	Cl_2	(PdO_2 + C)
	309–454	28.69 (28.743)	135	135.265	$C_7H_9N_3$	31.96 (31.514)
	454–1,000	24.22 (24.584)	114	115.69	C_8H_2O	

3.3. The stereochemistry and chemical reactivity prediction

To investigate the stereochemistry of the most stable structure of the complexes, it was focused first on the structure of the ligand, specifically on the orientation of its functional groups with respect to each other and with respect to the central azomethine (HC=N) part. The stereochemistry and chemical reactivity predictions of the ligand and its complexes were investigated by the hybrid density functional theory (DFT) method at the B3LYP level. The optimized structure of HL (Figure 2) showed that it has a planar arrangement with a C_1 point group and a total minimized energy of 16.52 kcal/mol. The dihedral angles N2−C10−C12−C14, C12−C10−C11−H28, and C7−C8−N20−O21 are equal to 180.0 °C, 180.0 °C, and −0.010 °C, respectively, confirming the planarity of the molecule. Also, the angles C9−N2−C10, C5−C9−N2, and O21−N20−O22 have the values 127.53 °C, 119.70 °C, and 123.46 °C, respectively. These values are corresponding to sp^2 hybridization and confirming that the molecule is nearly planar. The bond lengths of the azomethine moiety showed that the N2−C9 and N2−C10 bonds have the values 1.31 Å and 1.41 Å, respectively, suggesting double and single bond characteristics. These values are in the normal range observed before [21,36,37]. For example, the X-ray structure analysis of a Schiff base ligand derived from 2-phenylacetohydrazide and 2′-hydroxy acetophenone showed a value of 1.29 Å for the C=N of the azomethine part [21]. The optimized structure for HL showed the presence of hydrogen bonding between N2 and H23 (1.59 Å) to form an O(1)…H(23)…N(2) moiety. This bond separation illustrates the van der Waal displacement between H, the donor (D), and the acceptor (A). The orientation of the functional groups of the HL suggested that it might only coordinate to the metal ion through the nitrogen of the azomethine and the hydroxyl group, that is, it acts as a bidentate ligand with the coordination of NO set of donors.

The spectroscopic and analytical investigation of the cobalt and nickel complexes concluded that the metal ion bound to two L moieties and two coordinated water molecules. The energetically stable model of the nickel derivative showed a distorted octahedral geometry with a total minimized energy of 236.42 kcal/mol (Figure 2). The chelated ligand moiety to the Ni ion gave a six-membered ring. The bond lengths for the two Ni−N and the two Ni−O are 1.85 Å, 1.84 Å, 1.79 Å, and 1.80 Å, respectively. Optimized angles for the two N−Ni−O (six-membered cycles) are 92.32° and 85.02°. As shown from the figure,

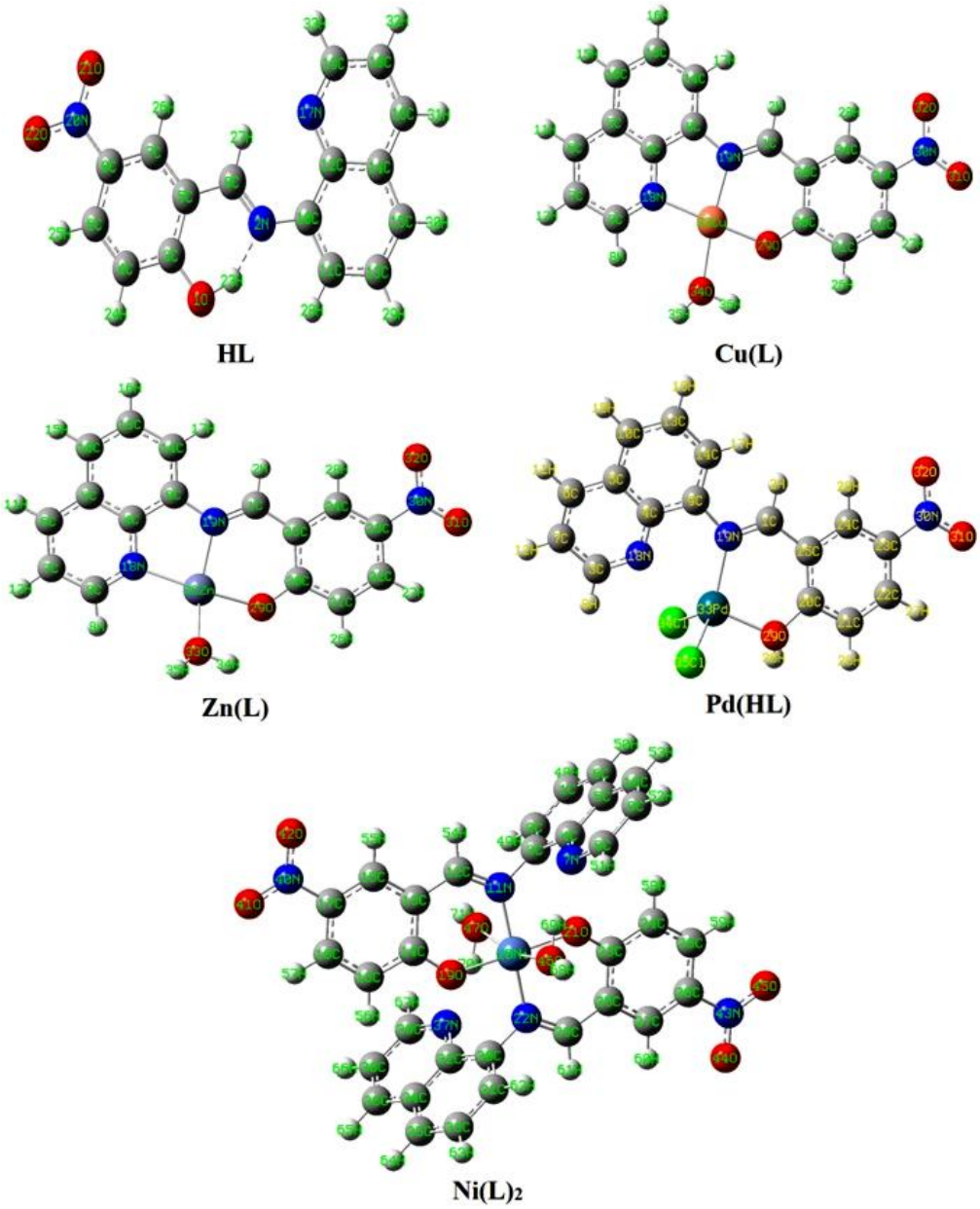

Figure 2: Voids concentration in lap joint versus Ti concentration.

the two coordinated water molecules are attached to the metal with a trans orientation and the O−Ni−O angle is 176.40°. The other bonds and angles of the complex are comparable to those of the ligand itself.

The optimized structures of the two complexes $[M(L)(H_2O)]^+$, M=Cu or Zn, were found to be almost identical (Figure 2). The metal existed in a distorted square-planar environment and the ligand bound to it in a tridentate fashion. The total minimized energy was 187.44 kcal/mol and 190.58 kcal/mol for the copper and zinc derivative, respectively. The dihedral angles of the planes containing the metal ion were C9−C4−N18−Cu33 = 1.74°, C3−N18−Cu33−O29 = 101.57°, C3−N18−Zn36−N19 = 176.53°, and C20−O29−Zn36−N18 = 76.65°. In addition, the bond angles between the metal ion and the adjacent atoms were N18−Cu33−N19 = 84.91°, O18−Cu33−O19 = 84.91°, O18−Cu33−O29 = 176.45°, N19−Cu33−O34 = 171.24°, O29−Cu33−O34 = 78.82°, N18−Zn36−N19 = 82.86°, O29−Zn36−O33 = 82.183°, N19−Zn36−O33 = 149.70°, and N19−Zn36−O29 = 93.35°. These data indicated the nonplanarity of the molecules as well as the distorted nature of their square planar arrangements. It can also be noted that in the zinc complex the two nitrogen atoms and the oxygen of the ligand moiety almost lie in the same plane with Zn, while the coordinated water molecule is out of the plane. The bond lengths between copper or zinc

Table 6: The global chemical reactivity descriptors for HL and its complexes.

Parameter	HL	$Ni(L)_2$	Cu(L)	Zn(L)	Pd(HL)
HOMO (eV)	−6.30	−5.93	−9.66	−9.41	−5.63
LUMO (eV)	−2.60	−2.68	−6.31	−6.19	−4.68
ΔE (eV)	3.70	3.25	3.35	3.22	0.95
X (eV)	4.45	4.31	7.98	7.80	5.16
V (eV)	−4.45	−4.31	−7.98	−7.80	−5.16
A (eV)	2.60	2.68	6.31	6.19	4.68
I (eV)	6.30	5.93	9.66	9.41	5.63
η (eV)	1.85	1.63	1.68	1.61	0.47
S (eV)	0.92	0.81	0.84	0.81	0.24
ω (eV)	5.36	5.70	19.01	18.87	28.02

and the coordinated donor atoms were in the normal ranges observed before for similar Schiff base complexes [21,38]. The values of bond separation for the copper derivative were found to be N18−Cu33 = 1.99 Å, N19−Cu33 = 1.97 Å, O29−Cu33 = 1.90 Å, and Cu33−O34 = 2.02 Å. On the other hand, the bond lengths for the zinc complex were N18−Zn36 = 2.0655 Å, N19−Zn36 = 2.0455 Å, O29−Zn36 = 1.9399 Å, and O33−Zn36 = 2.0516 Å.

In case of the $[Pd(HL)(Cl)_2]$ complex, the optimized structure showed that palladium species existed in a distorted tetrahedral skeleton with two coordinated chlorine atoms, and the ligand coordinated to it in a bidentate mode (Figure 2). The total minimized energy was 157.88 kcal/mol. From the figure, one can notice that the palladium metal and ligand moiety are nearly in the same plane, while the two chlorine atoms are out the plane in opposite positions. The distortion in the tetrahedral arrangement around the metal stemmed from the bond angles and dihedral angles. The calculated dihedral angles for the complex were Cl34−Pd33−Cl35 = 108.23°, C1−N19−Pd33−O29 = 12.44°, C20−O29−Pd33−Cl35 = 41.78° and C9−N19−Pd33−Cl34 = 72.53°. Also, the bond angles N19−Pd33−O29 = 106.64°, N19−Pd33−Cl34 = 112.12°, N19−Pd33−Cl35 = 108.88°, and O29−Pd33−Cl34 = 109.72° obviously deviated from regular tetrahedron. The bond lengths between palladium and nitrogen, oxygen and chlorine atoms were found to be N19−Pd33 = 1.952 Å, O29−Pd33 = 1.922 Å, and Pd33−Cl34 = 2.27 Å. They were in the normal range for these bonds as observed before [39,40]. For example, the palladium complex $[PdCl_2(L)]$, L = 2,6-diisopropyl-N-[(S)-pyrrolidin-2-ylmethyl]-aniline, exhibited Pd-N bond lengths equal to 2.04 Å and 2.07 Å, and Pd-Cl bond lengths equal to 2.31 Å and 2.32 Å [39].

The global chemical reactivity parameters including HOMO, LUMO, energy gap (ΔE), electronegativity (X), chemical potential (V), electron affinity (A), ionization potential (I), chemical hardness (η), chemical softness (S), and electrophilicity (ω) of the reported compounds are given in Table 6 [41]. The estimated frontier molecular orbital energies for the compounds are illustrated in Figure 3. The HOMO orbital energy represents electron donating ability, while the LUMO orbital energy characterizes electron withdrawing ability. The energy gap between them shows the molecular chemical stability. This parameter is crucial for determining molecular electrical transport properties. The smaller energy gap reflects the easiness of the CT, and the polarization, which occurs within the molecule [42]. Therefore, the order of increasing reactivity of the reported complexes is Pd(HL) > Zn(L) > $Ni(L)_2$ > Cu(L). The electronegativity parameter (X) is a reflection for the electrostatic potential, where the electron partially transferred from one of lower electronegativity to another of higher electronegativity [43]. The calculated data showed that the order of decreasing X is Cu(L) > Zn(L) > Pd(HL) > $Ni(L)_2$. On the other hand, the results of small chemical hardness values for the reported derivatives reflect the ability of charge-transfer within the molecule. The order of increasing the charge-transfer within the molecule is Pd(HL) < Zn(L) < $Ni(L)_2$ < Cu(L).

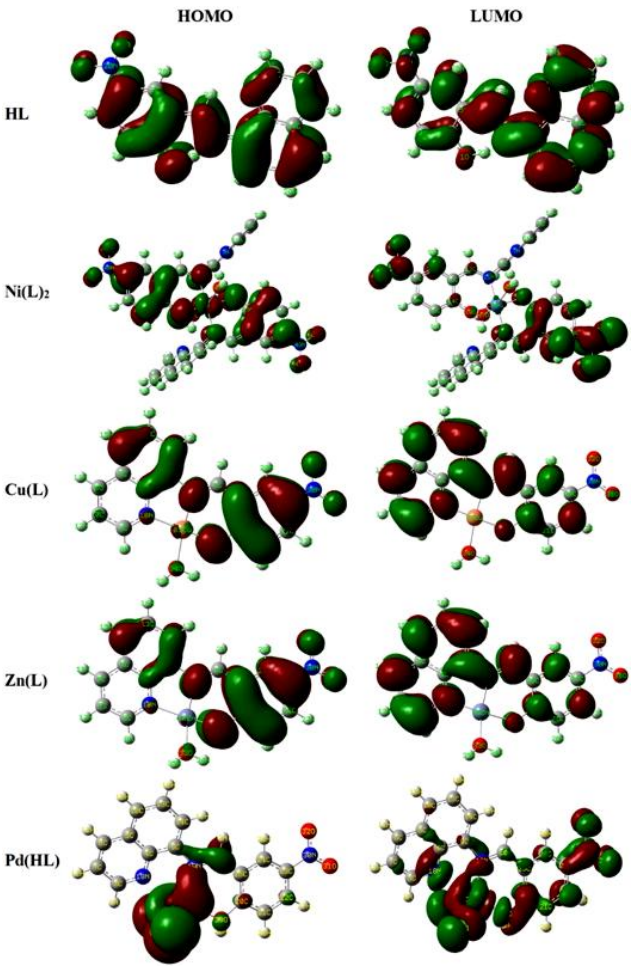

Figure 3: Joint strength (Mpa) versus Ti concentration (wt%).

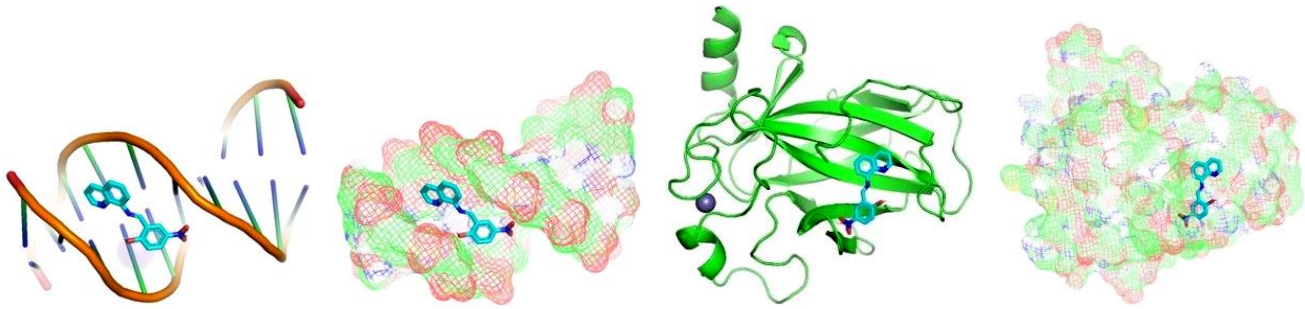

(a) (b) (c) (d)

Figure 4: 3D representation of HL interaction with: DNA ((a) cartoon; (b) mesh) and protein ((c) cartoon; (d) mesh).

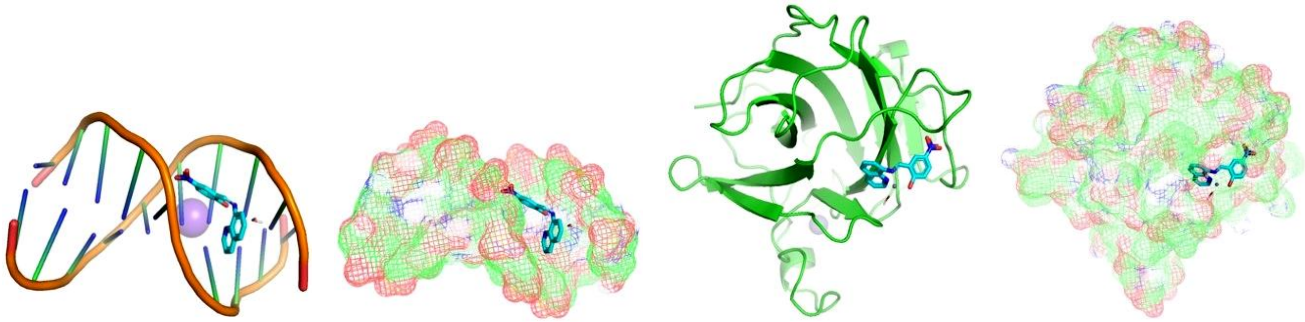

(a) (b) (c) (d)

Figure 5: 3D representation of zinc complex interaction with: DNA ((a) cartoon; (b) mesh) and protein ((c) cartoon; (d) mesh).

3.4. Biological activity

The in vitro antimicrobial activities of the ligand and its complexes were screened against four bacteria: *E. coli* and *E. aerogenes* as Gram-negative bacteria and *S. aureus* and *E. faecalis* as Gram-positive bacteria, and the fungus: *A. niger*. Surprisingly, the ligand and its palladium derivative showed only antibacterial activity towards *S. aureus*. The results indicated high antibacterial activities (inhibition zone: 26 mm for HL and 30 mm for Pd(HL)) and were found to be comparable with that of doxycycline standard (inhibition zone: 32 mm). Accordingly, it could be concluded that the Pd species improved the antibacterial activity relative to ligand. The high activity of the complex can be explained by the cell permeability concept and/or Tweedy's chelation theory [44,45,46]. According to the cell permeability concept, the metal ions can hardly pass through the membrane surrounding the cell due to the high polarity of such ions. On chelation, the polarity of Pd(II) ions can be reduced to a greater extent as a result of the overlap of the ligand and metal ion orbitals leading to a partial sharing of the positive charge of the metal ion with donor groups. Furthermore, the lipophilicity of complex is improved as the π-electron delocalization over the whole chelating ring increases. Subsequently, the penetration of the complex into lipid membranes will be enhanced and then blocking the Pd(II) binding sites in the enzymes of microorganisms.

3.5. Molecular docking of the HL and Zn(L)

Molecular docking is a useful tool to understand the interaction between the synthesized compounds and biological targets. Analysis of the docking data is used to predict the conformational changes associated with the amino acid residues at the binding position to accommodate the docked hydrophobic inhibitors. The HL ligand and its zinc complex were subjected to molecular docking studies using Auto Dock Vina 4 to understand the compound-DNA and compound-protein interactions and to explore the potential binding mode and energy. The docked ligands conformations were rated according to the binding energy, hydrogen bonding, and hydrophobic interactions between the two compounds (HL and Zn(L)) with either the B-DNA (PDB ID: 1ZEW) or the protein (PDB ID: 4MZI). The docking studies predict the way by which the docked compounds principally fit in the DNA or the protein minor grooves and how to involve of the hydrophobic, ionic, and hydrogen bonding interactions with the nitrogen bases. The binding interactions of HL and Zn(L) with the DNA and protein are displayed in Figures 4 and 5. The two derivatives

showed very good binding scores, which indicate high binding affinity between the receptors (DNA and protein) and ligand (HL and Zn(L)) molecules. These values display their high efficiency as bioactive compounds (-9.1 and -6.9 kcal/mol for HL, and -8.9 and -7.3 kcal/mol for Zn(L), resp.). In case of HL, the binding interaction with DNA comes from either hydrophobic interaction between the amino acid residues or hydrogen bonding with the DG 17 and DA 16 regions and the hydroxyl group of the ligand. On the other hand, the binding interaction of HL and protein comes from hydrophobic interaction and hydrogen bonds formed between HIS 193, HIS 214, and VAL 253 parts of protein. The Zn(L) derivative also showed similar interaction with both DNA and protein. Interestingly, the interaction of Zn(L) with DNA is comparable to that of HL due to the presence water OH groups instead of the hydroxyl group of ligand (interaction occurred between the nitrogen and water OH of Zn(L) with the DG 17, DG 19, and DA 6 regions). In addition, more binding interaction of Zn(L) with other sites of the protein were observed (VAL 143, ILE 232, ASN 200, ALA 159).

4. Conclusion

Spectroscopic investigations of some bivalent complexes of a molecularly designed Schiff base ligand derived from hydroxynitrobenzaldehyde and aminoquinoline revealed different structure features. The theoretical calculations based on DFT method confirmed the spectroscopic findings as well as gave information about the relative reactivity of the compounds. Molecular docking illustrated the possibility of the ligand and its zinc complex to interact with DNA.

Conflict of interest The fourth author is the Editor-in-Chief of this journal; accordingly, Dr. S. M. El-Medani and the coauthors were blind to the details of the review. The authors have no other conflicts of interest.

References

[1] L. H. Abdel-Rahman, N. M. Ismail, M. Ismael, A. M. Abu-Dief, and E. A. Ahmed, *Synthesis, characterization, DFT calculations and biological studies of Mn(II), Fe(II), Co(II) and Cd(II) complexes based on a tetradentate ONNO donor Schiff base ligand*, J Mol Struct, 1134 (2017), 851–862.

[2] R. G. Mohamed, A. A. Makhlouf, S. A. Mosad, A. A. Abdel Aziz, S. M. El-Medani, and R. M. Ramadan, *Spectroscopic, DFT, biological, DNA-binding, and antioxidant studies of some metal chelates with a novel thiazole-derived Schiff base*, J Coord Chem, 71 (2018), 3665–3688.

[3] X. W. Zhu, *Synthesis, crystal structures, and catalytic properties of dioxomolybdenum(VI) complexes derived from 4-chloro-2-{[4-diethylamino-2-hydroxybenzylidene]amino}phenol*, Russ J Coord Chem, 45 (2019), 532–538.

[4] R. M. Ramadan, W. M. Elsheemy, N. S. Hassan, and A. A. Abdel Aziz, *Synthesis, spectroscopic characterization, thermal behaviour, in vitro antimicrobial and anticancer activities of novel ruthenium tricarbonyl complexes containing monodentate V-shaped Schiff bases*, Appl Organomet Chem, 32 (2018), e4180.

[5] A. Jayamani, N. Sengottuvelan, S. K. Kang, and Y.-I. Kim, *Studies on nucleic acid/protein interaction, molecular docking and antimicrobial properties of mononuclear nickel(II) complexes of piperazine based Schiff base*, Inorg Chem Commun, 48 (2014), 147–152.

[6] D.-Y. Ma, L.-X. Zhang, X.-Y. Rao, T.-L. Wu, D.-H. Li, and X.-Q. Xie, *Synthesis, characterization, luminescence, antibacterial, and catalytic activities of a palladium(II) complex involving a Schiff base*, J Coord Chem, 66 (2013), 1486–1496.

[7] F. A. Beckford, J. Thessing, M. Shaloski Jr., P. C. Mbarushimana, A. Brock, J. Didion, et al., *Synthesis and characterization of mixed-ligand diimine-piperonal thiosemicarbazone complexes of ruthenium(II): Biophysical investigations and biological evaluation as anticancer and antibacterial agents*, J Mol Struct, 992 (2011), 39–47.

[8] Y. Li and Z. Zeng, *Synthesis, characterization and bioactivity of two rare-earth complexes with Schiff base from lysine-salicylaldehyde*, in Proceedings of the 2015 International Conference on Electronic Science and Automation Control, Atlantis Press, 2015, 1–4.

[9] N. Vamsikrishna, M. P. Kumar, S. Tejaswi, A. Rambabu, and Shivaraj, *DNA binding, cleavage and antibacterial activity of mononuclear Cu(II), Ni(II) and Co(II) complexes derived from novel benzothiazole Schiff bases*, J Fluoresc, 26 (2016), 1317–1329.

[10] S. N. Battin, *Vanillin-Aminoquinoline Schiff Bases and their Co(II), Ni(II) and Cu(II) Complexes*, Lulu Publication, North Carolina, USA, 2019.

[11] V. A. Shelke, S. M. Jadhav, V. R. Patharkar, S. G. Shankarwar, A. S. Munde, and T. K. Chondhekar, *Synthesis, spectroscopic characterization and thermal studies of some rare earth metal complexes of unsymmetrical tetradentate Schiff base ligand*, Arab J Chem, 5 (2012), 501–507.

[12] B. Rizwana and S. Santha Lakshmi, *Synthesis, characterisation and antimicrobial studies of Zn(II), Ni(II) and Cu(II) complexes of a Schiff base derived from o-vanillin and N-allyl thiourea*, Int J Chemtech Res, 4 (2012), 464–473.

[13] R. Suganthi, S. Santha Lakshmi, K. Geetha, and A. Abdul Rahuman, *Synthesis, spectroscopic characterisation, antimicrobial and larvicidal studies of some transition metal complexes derived from tetradentate Schiff base ligand*, J Pharm Res, 4 (2011), 4574–4576.

[14] S. Kumar, S. Bawa, and H. Gupta, *Biological activities of quinoline derivatives*, Mini Rev Med Chem, 9 (2009), 1648–1654.

[15] B. Bano, K. M. Khan, A. Jabeen, A. Hameed, A. Faheem, M. Taha, et al., *Aminoquinoline Schiff bases as non-acidic, non-steroidal, anti-inflammatory agents*, ChemistrySelect, 2 (2017), 10050–10054.

[16] K. Kaur, M. Jain, R. P. Reddy, and R. Jain, *Quinolines and structurally related heterocycles as antimalarials*, Eur J Med Chem, 45 (2010), 3245–3264.

[17] V. S. Zanon, J. A. Lima, T. Cuya, F. R. S. Lima, A. C. C. da Fonseca, J. G. Gomez, et al., *In-vitro evaluation studies of 7-chloro-4-aminoquinoline Schiff bases and their copper complexes as cholinesterase inhibitors*, J Inorg Biochem, 191 (2019), 183–193.

[18] H. F. Abd El-Halim, G. G. Mohamed, and M. N. Anwar, *Antimicrobial and anticancer activities of Schiff base ligand and its transition metal mixed ligand complexes with heterocyclic base*, Appl Organomet Chem, 32 (2018), e3899.

[19] P. R. Reddy, S. Rajeshwar, and B. Satyanarayana, *Synthesis, characterization of new copper (ii) Schiff base and 1,10 phenanthroline complexes and study of their bioproperties*, J Photochem Photobiol B, 160 (2016), 217–224.

[20] Q. Wei, J. Dong, P. Zhao, M. Li, F. Cheng, J. Kong, et al., *DNA binding, BSA interaction and SOD activity of two new nickel(II)*

complexes with glutamine Schiff base ligands, J Photochem Photobiol B, 161 (2016), 355–367.

[21] S. M. El-Medani, A. A. Makhlouf, H. Moustafa, M. A. Afifi, M. Haukka, and R. M. Ramadan, *Spectroscopic, crystal structural, theoretical and biological studies of phenylacetohydrazide Schiff base derivatives and their copper complexes*, J Mol Struct, 1208 (2020), 127860.

[22] R. M. Ramadan, A. K. Abu Al-Nasr, and O. A. M. Ali, *Synthesis, spectroscopic, DFT studies and biological activity of some ruthenium carbonyl derivatives of bis-(salicylaldehyde)phenylenediimine Schiff base ligand*, J Mol Struct, 1161 (2018), 100–107.

[23] R. M. Ramadan, A. K. Abu Al-Nasr, and A. F. H. Noureldeen, *Synthesis, spectroscopic studies, antimicrobial activities and antitumor of a new monodentate V-shaped Schiff base and its transition metal complexes*, Spectrochim Acta A Mol Biomol Spectrosc, 132 (2014), 417–422.

[24] M. J. Frisch, H. B. Schlegel, G. E. Scuseria, M. A. Robb, J. R. Cheeseman, G. Scalmani, et al., *Gaussian 09, Revision D.01*, Gaussian, Inc., Wallingford CT, 2009.

[25] O. Trott and A. J. Olson, *AutoDock Vina: improving the speed and accuracy of docking with a new scoring function, efficient optimization, and multithreading*, J Comput Chem, 31 (2010), 455–461.

[26] S. Emamzadah, L. Tropia, I. Vincenti, B. Falquet, and T. D. Halazonetis, *Reversal of the DNA-binding-induced loop L1 conformational switch in an engineered human p53 protein*, J Mol Biol, 426 (2014), 936–944.

[27] F. A. Hays, A. Teegarden, Z. J. Jones, M. Harms, D. Raup, J. Watson, et al., *How sequence defines structure: a crystallographic map of DNA structure and conformation*, Proc Natl Acad Sci U S A, 102 (2005), 7157–7162.

[28] W. L. DeLano, *The PyMOL Molecular Graphics System*, DeLano Scientific, San Carlos, CA, 2002.

[29] K. Nakamoto, *Infrared and Raman Spectra of Inorganic and Coordination Compounds: Part B: Applications in Coordination, Organometallic, and Bioinorganic Chemistry*, John Wiley & Sons, Hoboken, NJ, 6th ed., 2009.

[30] D. Kivelson and R. Neiman, *ESR studies on the bonding in copper complexes*, J Chem Phys, 35 (1961), 149–155.

[31] L. H. Abdel-Rahman and R. M. Ramadan, *Synthesis and characterization of some new mono- and binuclear copper(II) ternary complexes; X-ray crystal structure of copper(II)-N-(acetyl)phenylglycinate-imidazole ternary complex*, J Coord Chem, 60 (2007), 1891–1901.

[32] S. Chandra and K. Gupta, *Twelve-, fourteen- and sixteen-membered macrocyclic ligands and a study of the effect of ring size on ligand field strength*, Transit Met Chem, 27 (2002), 329–332.

[33] R. Foster, *Organic Charge-Transfer Complexes*, Academic Press, London, 1969.

[34] R. M. Ramadan, A. S. Attia, and M. F. El-Shahat, *Spectroscopic and electrochemical activity studies of some molybdenum chrysenesemiquinone complexes*, Polyhedron, 15 (1996), 301–307.

[35] T. Hatakeyama and L. Zhenhai, *Handbook of Thermal Analysis*, Wiley, Chichester, UK, 1998.

[36] M. Yıldız, O. Karpuz, C. T. Zeyrek, B. Boyacıoğlu, H. Dal, N. Demir, et al., *Synthesis, biological activity, DNA binding and anion sensors, molecular structure and quantum chemical studies of a novel bidentate Schiff base derived from 3,5-bis(triflouromethyl)aniline and salicylaldehyde*, J Mol Struct, 1094 (2015), 148–160.

[37] S. Hassen, H. Chebbi, M. F. Zid, and Y. Arfaoui, *Assembly and weak interactions in the crystal structure of 2-amino-4-(3-bromophenyl)-1,3,5-triazinobenzimidazolium chloride studied by X-ray diffraction, vibrational spectroscopy, Hirshfeld surface analysis and DFT calculations*, J Mol Struct, 1179 (2019), 678–684.

[38] J. T. Brewster 2nd, G. Anguera, M. D. Moore, B. S. Dolinar, H. Zafar, G. D. Thiabaud, et al., *Synthesis and characterization of a binuclear copper(II) naphthoisoamethyrin complex displaying weak antiferromagnetic coupling*, Inorg Chem, 56 (2017), 12665–12669.

[39] S. Nayab, H. I. Lee, and J. H. Jeong, *Dichlorido{2,6-diisopropyl-N-[(S)-pyrrolidin-2-ylmeth-yl]aniline-$\kappa^2 N, N'$}palladium(II)*, Acta Crystallogr Sect E Struct Rep Online, 69 (2013), m238–m239.

[40] B. J. Graziano, E. M. Collins, N. C. McCutcheon, C. L. Griffith, N. M. Braunscheidel, T. M. Perrine, et al., *Palladium complexes bearing κ^2-N, N and κ^3-N, N, O pendant amine bis(phenolate) ligands*, Inorganica Chim Acta, 484 (2019), 185–196.

[41] N. Raja, R. Ramesh, and Y. Liu, *Paramagnetic ruthenium(III) complexes bearing O,O chelating ligands: Synthesis, spectra, molecular structure and electron transfer properties*, Polyhedron, 31 (2012), 196–201.

[42] J. Zhang, X. J. Wang, Y. J. Yan, and W. S. Xiang, *Comparative studies on the interaction of genistein, 8-chlorogenistein, and 3′,8-dichlorogenistein with bovine serum albumin*, J Agric Food Chem, 59 (2011), 7506–7513.

[43] A. A. Abdel Aziz, F. M. Elantabli, H. Moustafa, and S. M. El-Medani, *Spectroscopic, DNA binding ability, biological activity, DFT calculations and non linear optical properties (NLO) of novel Co(II), Cu(II), Zn(II), Cd(II) and Hg(II) complexes with ONS Schiff base*, J Mol Struct, 1141 (2017), 563–576.

[44] N. A. Smith, P. Zhang, S. E. Greenough, M. D. Horbury, G. J. Clarkson, D. McFeely, et al., *Combatting AMR: photoactivatable ruthenium(ii)-isoniazid complex exhibits rapid selective antimycobacterial activity*, Chem Sci, 8 (2017), 395–404.

[45] D. W. Deamer, A. Kleinzeller, and D. M. Fambrough, eds., *Membrane Permeability: 100 Years since Ernest Overton*, vol. 48 of Current Topics in Membranes, Academic Press, San Diego, CA, 1999.

[46] B. G. Tweedy, *Plant extracts with metal ions as potential antimicrobial agents*, Phytopathology, 55 (1964), 910–914.